RESEARCH ARTICLE

Editor's Choice

Sheathed Molecular Junctions for Unambiguous Determination of Charge-Transport Properties

Lucia Herrer, Saman Naghibi, Ivan Marín, Jonathan S. Ward, Jose María Bonastre, S. J. Higgins, Santiago Martín, Andrea Vezzoli, Richard John Nichols,* José Luis Serrano,* and Pilar Cea*

Future applications of single-molecular and large-surface area molecular devices require a thorough understanding and control of molecular junctions, interfacial phenomena, and intermolecular interactions. In this contribution the concept of single-molecule junction and host-guest complexation to sheath a benchmark molecular wire–namely 4,4′-(1,4-phenylenebis(ethyne-2,1-diyl))dianiline – with an insulating cage, pillar[5]arene 1,4-diethoxy-2-ethyl-5-methylbenzene is presented. The insertion of one guest molecular wire into one host pillar[5]arene is probed by ^{1}H-NMR (nuclear magnetic resonance), whilst the self-assembly capabilities of the amine-terminated molecular wire remain intact after complexation as demonstrated by XPS (X-ray photoelectron spectroscopy) and AFM (atomic force microscopy). Encapsulation of the molecular wire prevents the formation of π-π stacked dimers and permits the determination of the true single molecule conductance with increased accuracy and confidence, as demonstrated here by using the STM–BJ technique (scanning tunneling microscopy– break junction). This strategy opens new avenues in the control of single-molecule properties and demonstrates the pillararenes capabilities for the future construction of arrays of encapsulated single-molecule functional units in large-surface area devices.

1. Introduction

Challenges in nano and supramolecular research have emerged from the interest in building nanoscopic devices[1] that are inspired by equivalent macroscopic functional homologous systems.[2–4] The combination of the drastic reduction in size with the appearance of new properties at the nanoscale have opened new avenues in the use of supramolecular materials,[5–8] with a number of nanodevices being described and developed for technological[9–11] or biological applications.[1,12] In the field of molecular electronics single molecule devices represent the ultimate miniaturization concept. These have evolved from the seminal paper from Aviram and Ratner,[13] which is a foundational work in the field of molecular electronics, and which proposed that molecular devices can act as electrical molecular rectifiers. There has been a renaissance of this area in recent years,[14] which has been boosted by promising applications beyond the initially envisioned one (electrical circuitry at the nanoscale), including single molecular sensing, thermoelectrics, heat transfer, spintronics, switching devices, and biomolecular electronics.[15–19]

Despite intense research in the areas of molecular electronics and single molecule devices some key challenges remain unsolved. Reproducibility in the conductance measurement is a recurrent problem in the single-molecule electronics field

L. Herrer, J. M. Bonastre, S. Martín, P. Cea
Departamento de Química Física
Facultad de Ciencias
Universidad de Zaragoza
Zaragoza 50009, Spain
E-mail: pilarcea@unizar.es

L. Herrer, I. Marín, J. M. Bonastre, S. Martín, J. L. Serrano, P. Cea
Instituto de Nanociencia y Materiales de Aragón (INMA)
CSIC-Universidad de Zaragoza
Zaragoza 50009, Spain
E-mail: joseluis@unizar.es

L. Herrer, J. M. Bonastre, S. Martín, P. Cea
Laboratorio de Microscopias Avanzadas (LMA)
Universidad de Zaragoza
Zaragoza 50018, Spain

S. Naghibi, J. S. Ward, S. J. Higgins, A. Vezzoli, R. J. Nichols
Department of Chemistry
University of Liverpool
Crown Street, Liverpool L69 7ZD, UK
E-mail: nichols@liverpool.ac.uk

I. Marín, J. L. Serrano
Departamento de Química Orgánica
Facultad de Ciencias
Universidad de Zaragoza
Zaragoza 50009, Spain

**ADVANCED
SCIENCE NEWS**
www.advancedsciencenews.com

**ADVANCED
MATERIALS
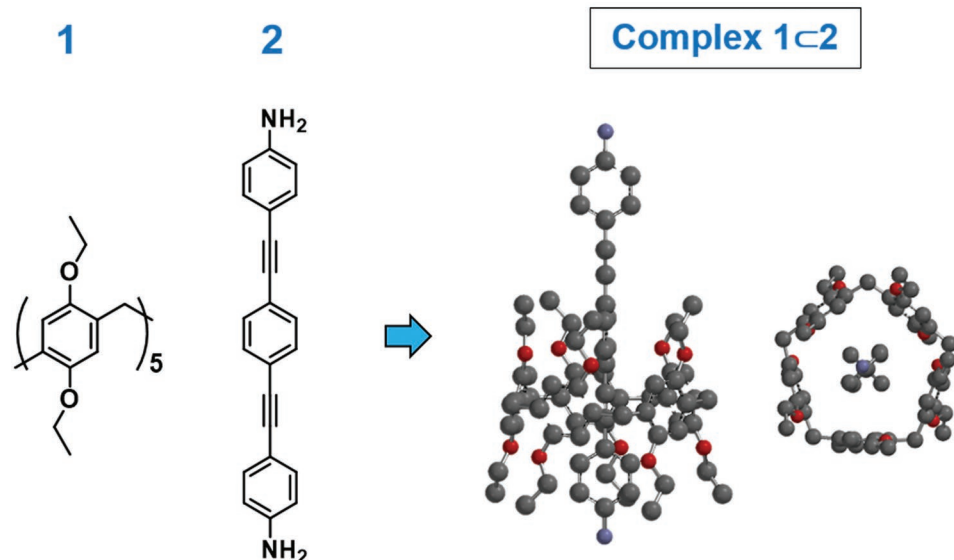INTERFACES**
www.advmatinterfaces.de

Figure 1. Chemical structure of compounds **1** and **2**, and molecular models for the host-guest complex **1⊂2**.

for several reasons,[20–28] with a key one being the formation of multi-molecular junctions. Formation of multi-molecular junctions can result in a distribution in several conductance values and, eventually, loss of the desired single-molecule functionality of the device. Interactions between neighboring molecules may also result in differing behavior of molecules embedded in large molecular area devices as compared to their single molecule counterparts.[29] The optimal situation for the unequivocal measurement of the electrical properties of a single molecule junction involves disperse, non-interacting molecules, that assemble one at a time in the break-junction nanogap. This can however be difficult to attain both in solution[30,31] and in "dry" measurements (in air or vacuum).[32] Significant variations in the measured conductance of purportedly single-molecule junctions have been observed when the experiments are performed at different concentrations, accompanied by dramatic effects on the stability of the fabricated junctions.[33]

The foregoing discussion highlights that new approaches are needed for conductance measurements on molecular junctions and the subsequent fabrication of molecular devices, with the clear need to reduce the influence of intermolecular interactions. A possible solution to these problems is to provide each molecular wire with an insulating "sheath". The sheath inhibits both intermolecular effects by uniformly spacing the molecular wires deposited on a surface or within the device. This prevents formation of multimolecular junctions, with the single molecule configuration being thereby preferred. This concept turned our attention to host-guest chemistry, as there are a wide variety of systems that have been used as a host for active molecules resulting in supramolecular complexes for a wide range of applications.[34–38] Among host molecules, pillar[n]arenes[39,40] represent a widely explored material for a number of reasons: 1) Their potential use as chemical sensors based on host-guest mechanisms, with examples including the detection and separation of volatile organic solvents or air pollutants,[41,42] selective adsorption and sensitive detection of metal ions,[43,44] and supramolecular networks for light

modulation,[45] thereby giving rise to an extensive range of applications.[46–57] 2) Pillar[n]arenes are synthetically easy to functionalize on their upper and lower rims;[58] last but not least 3) they spontaneously arrange themselves in layers, and are readily deposited on surfaces.[59–61]

A large number of compounds have been reported to act as cavity guests inside pillar[5]arenes.[52,62–64] In addition, there are a few examples in the literature of host-guest complexes in molecular electronics, using different macrocycles. In 2012, Kiguchi et al.[65] studied the single molecule conductance of a π-conjugated rotaxane by STM break junction, finding a suppression of conductance fluctuations by covalently encapsulating a molecular wire with a cyclodextrin. Single molecule conductance of host-guest complexes composed of cucurbituril and viologen moieties, was studied by STM formed molecular junctions (using the *I(s)*-STM technique), showing that robust junctions could be formed for viologen molecules located within nano-sized molecular cavities.[66] Viologens were also shown to be efficiently complexed by crown ethers, with an overall reduction of intramolecular coulombic repulsion.[33] In 2019 Tang et al.[67] demonstrated that the single molecule conductance of organoplatinum(II) metallocycle hosts can be enhanced by an order of magnitude by the inclusion of a C_{60} guest molecule. Very recently, Wang et al.[68] showed the gating effect of cation-π interaction in a viologen-pillar[5]arene host-guest complex. Other examples of molecular manipulation at the single molecule level that make use of host-guest interactions include the positioning of molecules or host-guest assemblies within nanogaps between surfaces and plasmonic nanoparticle top contacts.[69,70] These platforms could be used in a number of applications such as single-photon emitters, photon blockades, non-linear optics and reactions triggered at the single molecule level. Moreover, understanding how host-guest complexes behave at the single molecule level not only opens new avenues for a better understanding of supramolecular chemistry but also could provide precise control of the local environment in molecular assembles to create

nano-environments for better control of molecular properties at the nanoscale.

In this contribution, we focus our efforts on the complex illustrated in **Figure 1**. This comprises a host compound, pillar[5]arene, bearing ten ethoxy groups in the 2 and 5 position of the aromatic rings (compound **1**), and a guest material, which is an amine-terminated OPE (oligophenyleneethynylene) with amine termini at both ends (4,4′-(1,4-phenylenebis(ethyne-2,1-diyl))dianiline, (compound **2**) which enables the fabrication of single-molecule junctions. Importantly, the host pillar[5]arene is unfunctionalised so that it does not interact with the metallic electrodes and acts only as a non-conductive sheath for the encapsulated single molecular wire. Primary amines are well-known anchoring groups that form molecular junctions with a variety of different metal contacting electrode, thus facilitating the electrical and spectroscopic characterization of the complexes and comparison with the pure compound.[71,72] In what follows, it is demonstrated that i) the pillar[5]arene used here (compound **1**) is able to act as a supramolecular host for an OPE derivative (compound **2**). ii) the complex maintains the self-assembly properties of the guest molecule and iii) the host can be used as a "molecular sheath" to suppress the formation of dimeric junctions, insulating the single-molecule wire and preventing it from interacting with its neighbors.

2. Results and discussion

The synthesis of compound **1**, **2** and the **1⊂2** complex is described in the Supporting Information (section 1, with Figures S1, S2, Supporting Information showing the NMR of compounds **1** and **2**). The formation of the **1⊂2** complex was studied by ^{1}H-NMR (**Figure 2**). All the signals corresponding to the protons in the complex **1⊂2** are clearly visible in the spectra, Figure 2a), showing signals at δ ppm, 7.43 (s, 4H), 7.35 (d, J = 8.7 Hz, 4H), 6.71 (s, 10H), 6.65 (d, J = 8.7 Hz, 4H), 3.83 (q, J = 6.8 Hz, 20H), 3.77 (s, 10H), 1.27 (t, J = 6.8 Hz, 30H). The relative intensities of the signals reveal a 1:1 stoichiometry.

As can be seen in Figure 2a,b, a small downfield chemical shift is observed in the signals corresponding to the *l*, *j*, and *i* protons of compound **1** upon complexation. A more significant variation is observed in the mobile amine protons of compound **2**. As can be seen in Figure 2a,b, these protons appear at 3.83 ppm in the spectrum of compound **2**, whereas in the NMR spectrum of the complex this signal becomes broader and it is not clearly visible. It is important to take into account that the signal at 3.7 ppm corresponds to 30 protons attributable to the *j* and *k* protons of the pillararene moiety.

A key aim of this work is that the **1⊂2** complex forms molecular junctions, which requires good coordination of compound **2** between a pair of gold electrodes. In other words, compound **2** must be bonded to both the bottom gold substrate and to the gold-tip of the STM to form a robust molecule junction. It is therefore necessary to evaluate the surface bonding properties of the **1⊂2** complex on a gold surface. X-ray Photoelectron Spectroscopy (XPS) was used to evaluate this for a self-assembled monolayer (SAM) of **1⊂2** on gold (see the experimental section for the SAM preparation). **Figure 3** shows the N1s region for

the powder of **2** as well as the SAM of **1⊂2**. Whilst the powder of **2** shows a single N peak at 399.5 eV, attributed to the terminal free amines, the SAM of **1⊂2** shows a N1s peak which can be deconvoluted into two separate peaks at 399.7 and 400.4 eV, corresponding to the free amine of **2** oriented towards the upper part of the monolayer, and to the amine bonded to the gold surface of the substrate, respectively.[71] Additionally, the peak integration ratio of these to N1s peaks is ca. 1:1 which is in good agreement with half of the −NH$_2$ terminal groups bonded to the electrode whilst the other half −NH$_2$ terminal groups remain free (the slightly higher value for the −NH$_2$ free terminal groups is due to the high sensitivity of the XPS spectrum to the location of the involved atom within the film, and in this case the external nitrogen atom in the unbonded −NH$_2$ group results in a slightly higher integrated peak as compared to the inner nitrogen atom from the amine group chemisorbed to the gold surface[27]). This result demonstrates that the complex **1⊂2** is chemisorbed onto the gold substrate through one of the terminal amine groups of **2**.

In order to obtain further evidence for the assembly of **1⊂2** monolayers on the gold electrode, an atomic force microscopy (AFM) lithography method[73] was used to scratch through the SAM of **1⊂2** with the AFM tip (see section 2 in the Supporting Information). Using this procedure, a thickness for the **1⊂2** complex monolayer of 1.81 ± 0.07 nm was obtained. Importantly, the thickness of the SAM is in agreement with the theoretical value calculated with the Spartan'14 V.1.1.4. software, assuming that the length of the complex equals the length of the guest molecule, i.e., 1.98 nm for compound **2**. The thickness of **1⊂2** monolayers (1.81 ± 0.07 nm) is larger than the thickness of **1** monolayers (1.27 nm ± 0.33 nm) and similar to (or slightly higher than) the thickness of **2** monolayers (1.78 ± 0.14 nm), which is an indication of the presence of the **1⊂2** complex, when taken together with the deductions from AFM on the surface (otherwise films with areas showing two different thicknesses or at least an averaged thickness between those of **1** and **2** would have been obtained). Taking together the data provided by the XPS and AFM experiments, it can be concluded that compound **2** is chemisorbed onto the gold electrode and it is also inserted into the pillararene cavity of compound **1**, following the deposition of the **1⊂2** complex on the bottom electrode.

Having established the suitability of **2** for efficient encapsulation by **1** and the capability of the **1⊂2** complex to form monolayers on gold surfaces, we then performed the single-molecule charge transport characterization by using the scanning tunneling microscopy–break junction (STM-BJ) technique.[74] In this technique, a metallic point contact is fabricated between a Au STM tip and a Au substrate by driving the two together with a piezoelectric transducer. After reaching conductance values ≫ $5G_0$ (where G_0 is the quantum of conductance ≈ 77.48 µS) the two electrodes are pulled apart at a relatively slow speed (20 nm s$^{−1}$) to rupture the Au-Au contact and create a nanogap where molecules can self-assemble and form a metal-molecule-metal junction. The molecular junction is then stretched until rupture occurs. The process is performed with a bias *V* applied between the substrate (source) and the tip (drain) in the dynamically formed two-terminal device configuration, and the current *I* flowing through the junction
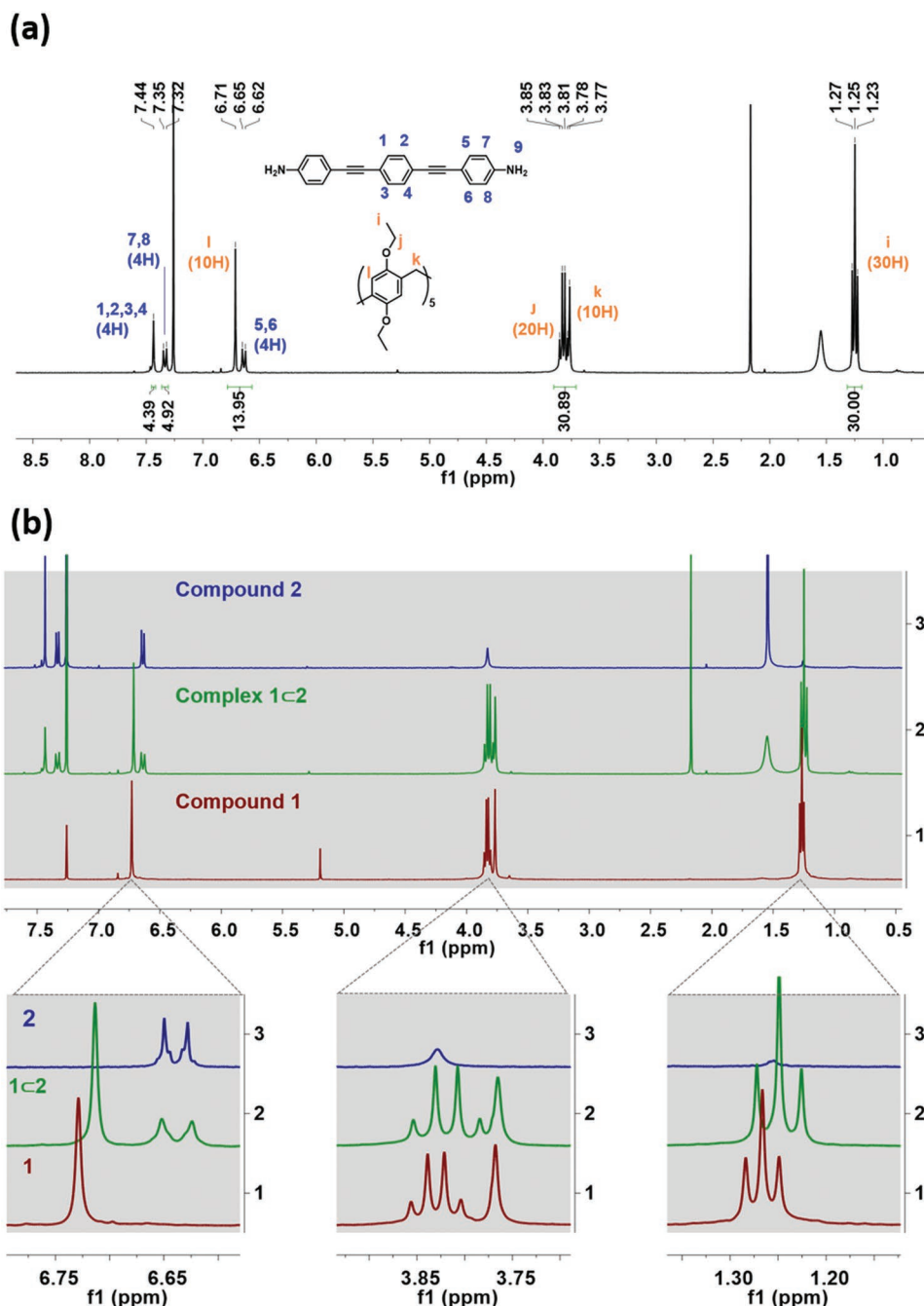
**ADVANCED
SCIENCE NEWS**
www.advancedsciencenews.com

**ADVANCED
MATERIALS
INTERFACES**
Open Access
www.advmatinterfaces.de

Figure 2. a) ^{1}H NMR of complex **1⊂2** (400 MHz, CDCl₃). b) Comparison between the ^{1}H NMR spectra of the compounds **1** and **2** and complex **1⊂2** spectra in CDCl₃. c) Enlarged sections of b) highlighting the chemical shifts.

is monitored as a function of the electrode relative position. Several thousand junction formation and breaking cycles are performed, and the obtained current-distance traces are compiled in conductance ($G = I/V$) histograms showing conductance peaks. 2D conductance versus electrode separation maps are constructed, where the distribution of conductance values versus junction stretching distance is visualized by the boldly colored high-density regions.

It is well known that aromatic conjugated molecular wires have a tendency to stack and form dimeric junctions in

which each monomer can be bound to the electrodes through only one of their termini (**Figure 4**a). In such stacked and staggered configuration charge tunnels through the eigen-channel opened by the efficient π-π interaction between the two face-to-face molecules. The effect has been observed for oligophenylenes,[75] imidazoles,[76] (oligo)thiophenes,[77] and, particularly relevant to this study, oligophenyleneethynylenes (OPEs).[78,79] The eigenchannel opened by the π-π interaction is generally less transparent to tunneling than interatomic bonds, and charge transport through stacked dimers

**ADVANCED
SCIENCE NEWS**

www.advancedsciencenews.com

**ADVANCED
MATERIALS
INTERFACES**
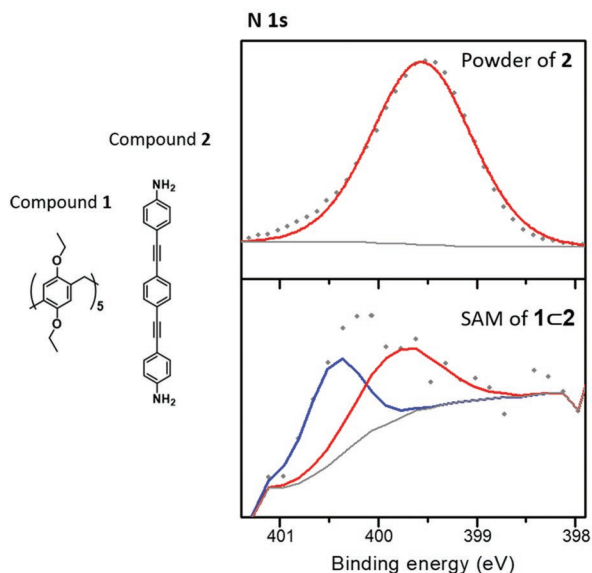
www.advmatinterfaces.de

Figure 3. XPS spectra of the powder of compound **2** (upper) and for the **1⊂2** SAM complex in the N1s region (lower).

is associated with lower conductance values than the corresponding single-molecule junctions.

The formation of stacked junctions was favored in STM-BJ experiments performed in air on a sub-monolayer of **2** deposited on the Au substrate by incubating it for 1 h in a 1 mM acetone solution. As can be observed in Figure 4c, this resulted in a strong contribution from the π-stacked junction, as the most intense peak in the 1D conductance histogram centered at ≈$10^{-5.3}$ G_0 in addition to a secondary peak at the higher conductance of ≈$10^{-4.2}$ G_0. The latter was confirmed to correspond to the single-molecule conductance by repeating the measurements in a solvating environment (a mixture of mesitylene and tetrahydrofuran 4:1 v:v) where the formation of stacked dimers is hindered by the presence of a solvent shell surrounding the molecular wire. Here, only a single conductance peak at ≈$10^{-4.2}$ G_0 is present in the 1D histogram (Figure 4c, shaded gray). The signal for the stacked dimer (the lower plateau in Figure 4e), after addition of the gold electrode snapback of 0.65 nm,[81] extends to electrode separations larger than the length of the molecule (Figure 4e). This extension beyond the length of a single molecule clearly demonstrates its supramolecular character and consequently the lower plateau is attributed to the stacked dimer. The same set of measurements performed on a substrate incubated for 1 h in an equimolar solution of **1** and **2** resulted in the single-molecule conductance peak only (Figure 4d) and similarly its conductance versus electrode separation density map did not show significant features extending beyond the molecular length of **2** (figure 4f). Therefore, encapsulation of **2** in **1** gives an overwhelming propensity for single molecule junctions by preventing π-stacking through **1⊂2** complex formation.

To further confirm the supramolecular nature of the junctions made with **2** in air arising from the π-stacking, we performed flicker noise analysis on these fabricated junctions. In this technique, the current signal of molecular junctions is
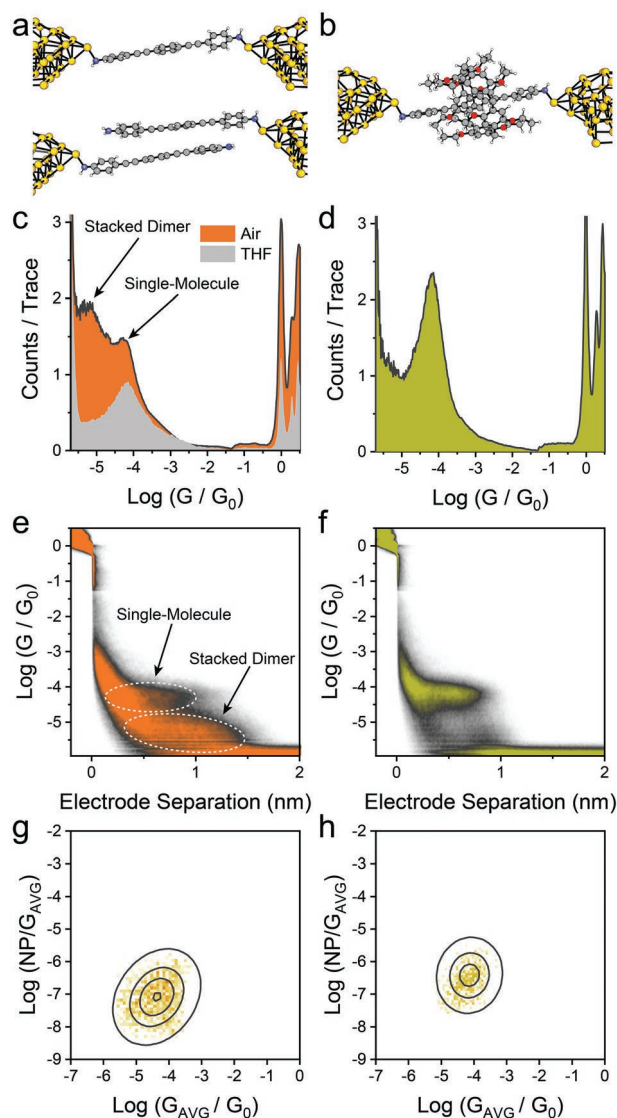

Figure 4. STM-BJ studies. a) Idealized structure of a single-molecule junction of **2** (top) and its stacked dimer (bottom) also (b) with an idealized structure in which the molecular wire is assumed to be symmetrically placed within the host molecular cage to form the **1⊂2** supramolecular complex junction. c) 1D conductance histogram of **2** measured in air, 200 mV bias (orange) and in mesitylene:tetrahydrofuran 4:1 (grey). d) 1D conductance histogram for the **1⊂2** complex measured in air, 200 mV bias. e) Conductance – electrode displacement density map for **2** in air. f) Conductance – electrode displacement density map for **1⊂2** in air. g) PSD flicker noise analysis for **2**. h) PSD flicker noise analysis for the **1⊂2** complex. Histogram and density map in c) and e) compiled from 5209 traces with no data selection. Histogram and density map in d) and f) compiled from 5209 traces with no data selection. Histogram for **2** in THF c) normalized at 0.5 counts/trace to avoid overlapping with the histogram obtained in air. Flicker noise heatmaps in g) and h) compiled from respectively 12 706 and 15 282 traces using the data analysis routine described in our previous publication on the subject.[80] Colors in a) and b): C = gray, N = blue, H = white, O = red, Au = yellow. Dashed contours in e) as guide to the eye. Solid contours in g) and h) are the 25%, 50%, and 75% height of the 2D Gaussian fit to the map.

analyzed in the frequency domain, and the noise power is calculated by integrating the power spectral density between 100 Hz

**ADVANCED
SCIENCE NEWS**

www.advancedsciencenews.com

**ADVANCED
MATERIALS
INTERFACES**

www.advmatinterfaces.de

and 1 kHz. The noise power follows a power law dependence of the conductance ($NP \propto G^n$), with the scaling exponent n being close to 1 when charge transport is purely through-bond. This scaling exponent increases toward 2 when charge transport has a through-space component. As an example, in a terphenyl molecular wire, the scaling component associated with the single-molecule junction was found to be 1.16, increasing to 1.78 for its stacked dimeric junction.[82] To acquire data significant to this analysis, we performed a "pull and hold" STM-BJ experiment, where the tip is retracted in a step-like manner, and its position relative to the substrate is held stable for 100 ms between each step. The junction current is recorded at high speed (100 000 samples s^{-1}), sliced between steps and fed to an automated algorithm for data selection, average conductance G_{AVG} calculation, and fast Fourier transform (FFT) analysis. Details on the instrumentation and the data analysis procedures can be found in our previous publication on the subject.[80] The results for **2** are presented in Figure 4g as normalized noise power versus average conductance in order to analyze their correlation. While in this plot the contributions from the stacked dimer and the single-molecule junction cannot be distinguished as they lie too close in conductance, the overall noise power follows the power law dependence with a scaling exponent of 1.55 (obtained by finding the value of n at which the Pearson's correlation coefficient between NP/G_{AVG}^n and G_{AVG} is minimized), indicating significant contribution from through-space coupling. Repeating the same experiment on **1⊂2** (Figure 4h) gave a reduced scaling coefficient of 1.21, consistent with single-molecule through-bond transport (see Supporting Information for normalized heatmaps).

To further verify the proposed "molecular sheath" behaviour of the pillar[5]arene, we turned our attention to another class of molecular wires that are known to form robust dimeric junctions. Oligothiophenes are reported in the literature as being able to form robust dimer junctions with high probability even in solvating environment,[77] and they are therefore the ideal candidates for our study, as a control experiment. The dimeric nature of the junctions was confirmed by flicker noise measurements, which reported high scaling coefficients (e.g., >1.5) for the whole family of oligothiophene-based wires. We performed STM-BJ experiments on 5-(4-(methylthio)phenyl)-2,2″:5″,2‴-terthiophene (compound **3**, structure shown in **Figure 5**) under the same conditions reported by Li et al. (1 mM in mesitylene:THF 4:1) and we were able to reproduce the observed behavior.[77] **3** can form robust dimeric junctions with remarkably high charge transport efficiency. Performing the same experiment in the presence of an equimolar amount of the pillar[5]arene, however, resulted in an almost complete suppression of junction formation, with no evidence of π-stacking dimerisation of **3** within our experimental window. This result is in agreement with the observations of Hua et al.[83] who observed clear supramolecular association between thiophene and pillararenes. We further confirmed that the observed behavior was due to encapsulation of **3** rather than by pillar[5]arene-Au interactions disrupting junction formation by performing another control experiment, where a two-fold excess of **3** was present in solution (thereby ensuring some non-encapsulated material would be available to form stacked junction). In this control experiment, the results of
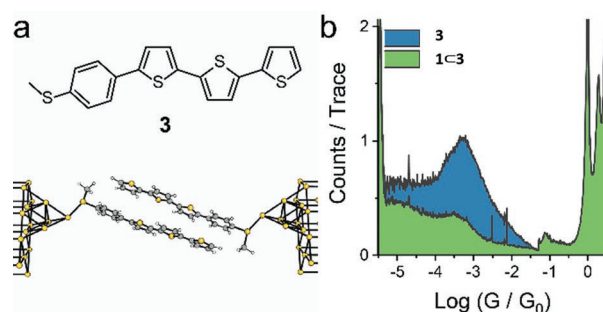

Figure 5. Control Experiment: a) Structure of the compound **3** (top) and its stacked dimer junction (bottom). b) 1D conductance histogram of **3** and the complex **1⊂3** (as equimolar solution in mesitylene:tetrahydrofuran 4:1 v:v) at 200 mV bias. Histogram in b) compiled from 4841 (**3**) and 4733 (**1⊂3**) traces, with no data selection.

which are available in the Supporting Information, the formation of stacked junction is indeed recovered, contributing to a peak in the conductance histogram.

Overall, our results suggest that while encapsulation with a pillar[5]arene does not change significantly the overall junction conductance, such encapsulation significantly affects the ability to form stacked dimers.

3. Conclusions

In this contribution a molecular wire (compound **2**) has been encapsulated into a molecular cage (compound **1**) to form a host-guest complex. The host-guest complex preserves the self-assembling capabilities of the molecular wire and is shown to form self-assembled monolayer films on gold, which have been characterized by XPS and AFM lithography. This propensity to self-assemble into monolayer films opens up new opportunities for the formation of large area molecular junctions of defined host-guest complexes. The electrical properties of the host-guest complex in air (**1⊂2**) have been determined using the STM-BJ method. The conductance of **1⊂2** has then been compared with that of the bare molecular wire, **2**. These results clearly demonstrate that the encapsulation of the molecular wire does not result in a change in the electrical properties but, importantly, encapsulation prevents the formation of stacked dimers. Therefore, this encapsulation strategy enables the determination of "true" *single-molecule* conductance by sterically inhibiting the formation of multi-molecular junctions. The surface analysis of the **1⊂2** complex within the self-assembly films (with XPS confirming the presence of free amines and amines chemisorbed onto the gold substrate, and AFM determining of a film thickness compatible with the **1⊂2** complex) together with the electrical characterization (conductance value identical to the free molecular wire and suppression of the signal for the stacked dimer) are indicative of a complete insertion of the molecular wire into the pillararene cavity with free access from both terminal groups of the molecular wire in the complex to both electrodes. Additionally, this encapsulation strategy also opens the path for the formation of large area molecular devices that are composed of extended arrays of single-molecule functional units which are individually shielded from their neighbor

**ADVANCED
SCIENCE NEWS**

www.advancedsciencenews.com

**ADVANCED
MATERIALS
INTERFACES**

www.advmatinterfaces.de

molecules. Future work will be devoted to assessing the suitability of other molecular compounds to encapsulate and "insulate" functional molecules from surrounding molecules. Exploitation of the template capabilities of hosts is a further attractive possibility.

4. Experimental Section

Synthesis of compounds **1** and **2** was adapted from previously reported procedures (see Supporting Information section 1). All chemicals were used as received, with the exception of 1,4-diethynylbenzene which was purified by sublimation before its use. Gold-on-glass substrates were purchased from Arrandee and flame annealed prior to use. Gold-on-mica samples were purchased from Georg Albert PVD-Coating. Mica substrates were purchased from Ted Pella Inc. V1 quality.

NMR characterization was performed in Bruker AV-300, Bruker AV-400 and Bruker AV-500. Mass Spectra were registered in a Bruker Microflex equipped with a MALDI+/TOF spectrometer and a nitrogen laser of 337 nm. Ditranol was the matrix in all cases. A Varian Cari 50 Bio spectrophotometer with a dual beam and a Czerny-Turner monochromator was used for UV-vis characterization. Imaging and scratching on samples were registered in ambient air conditions with a Multimode 8 from Veeco-Bruker equipped with a Nanoscope V control unit in Tapping and Contact modes. RTESPA-150 AFM probes (90-210 kHz, 1.5-10 N m^{-1} and nominal radius of 8 nm) were used and purchased from Bruker. AFM nanolithography ("nano-shaving or scratching") was achieved in contact mode (scan rate 3 Hz) by selecting a high deflection set point ($\approx$2 V) in order to apply a high force (higher than 100 nN) onto the sample and thereby remove the organic material. The RMS (root mean square) roughness, surface coverage and height/depth statistical analysis were obtained using the Nanoscope V.1.40 software. XPS spectra were recorded on a Kratos AXIS ultra DLD spectrometer equipped with an Al Kα X-ray monochromatic source (1486.6 eV) and using 20 eV as pass energy. Binding energies were calibrated according to the C1s peak at 284.6 eV.

Self-assembled monolayers of the **1⊂2** complex for XPS and AFM experiments were prepared by immersing the substrate (gold on glass or mica) for 24 h into a 0.5 × 10^{-4} M solution in MeOH:CHCl$_3$ solvent mixture (1:1, v/v) at 20 °C. The solution was sonicated for 20 min before substrate incubation to ensure that no aggregates were formed in solution prior to the SAM formation. After incubation, the sample was thoroughly rinsed with the solvent mixture and dried with a N$_2$ flow.

STM-BJ experiments were performed with a modified commercial system (Keysight Technologies 5500 SPM). Two different current-voltage converters: a custom-built[84] low-bandwidth, four-channel amplifier for wide dynamic range measurements, and a high-bandwidth commercial amplifier (Femto DLPCA-200) for high-speed acquisition and flicker noise analysis were used. The piezo transducer and bias of the STM were controlled by an arbitrary waveform generator (Keysight Technologies 33522B), and data acquisition was performed with a National Instruments PXI system (PXIe-1062Q chassig PXIe-4464 DAQ PXIe-PCIe8381 controller). All signals were routed in and out of the STM through a break-out box (Keysight Technologies N9447A). STM tips freshly cut from a spool of Au wire (Goodfellow Cambridge, 0.25 mm dia, 99.999+%) was used and gold-on-mica substrates ($\approx$200 nm of Advent Research Materials 99.99+% Au deposited on freshly cleaved Agar Scientific Muscovite Mica with an Edwards E306A evaporator). STM tips were mechanically annealed[85] before starting the data acquisition process. Substrates were thermally annealed with a butane micro-torch before use. Dry, analytical grade Fisher Scientific acetone was used during sample preparation. The experiments in liquid environment were performed with Tokyo Chemical Industry mesitylene (98%) and Fisher Scientific tetrahydrofuran. The latter was dried by passing it through an alumina column and stored over molecular sieves (4 Å) under a N$_2$ atmosphere until use. Data analysis was performed with bespoke algorithms written in Python 2.7 and National Instruments Labview 2022. A detailed description of the instrument used and the data analysis routines was available in our recent publications.[80,86]

Supporting Information

Supporting Information is available from the Wiley Online Library or from the author.

Conflict of Interest

The authors declare no conflict of interest.

Author Contributions

L.H., S.N., and I.M. contributed equally to this work. L.H. and I.M. did the synthesis and characterization of compounds **1**, **2** and the **1⊂2** complex. J.M.B. contributed to the NMR characterization and interpretation of compounds **1**, **2** and the complex as well as to the monolayer preparation. L.H. also prepared the films for AFM and XPS characterization. S.N. did the STM-BJ measurements. A.V. also contributed to the measurement and interpretation the STM-BJ results. J.S.W. performed and reported the synthesis and characterisation of compound under the supervision of S.J.H. S.M. worked on the XPS and AFM studies. A.V. R.J.N, J.L.S., and P.C. conceptualized this investigation, supervised the experimental work and they wrote the manuscript with the contribution of all authors.

Data Availability Statement

The data that support the findings of this study are openly available in Library of Liverpool University at https://doi.org/10.17638/datacat.liverpool.ac.uk/1960, reference number 1960.

[1] N. Salahuddin, A. Galal, Chapter 4 – Improving chemotherapy drug delivery by nanoprecision tools, in *Nanostructures for Cancer Therapy*, (Eds: A. Ficai, A. M. Grumezescu), Elsevier, **2017**, pp. 87–128.

[2] *Calixarenes and Beyond*, (Eds: P. Neri, J. L. Sessler, M.-X. Wang, Springer, **2016**, Cham.

[3] Molecular and Supramolecular Devices, in *Supramolecular Chemistry*, **1995**, pp. 89-138.

[4] Applied Nanotechnology, 2nd Edition, (Ed: J. J. Ramsden), **2014**, William Andrew Publishing, Oxford.

[5] D. Sluysmans, J. F. Stoddart, *Trends in Chem.* **2019**, *1*, 185.

[6] A. Sebastian, M. Le Gallo, R. Khaddam-Aljameh, E. Eleftheriou, *Nat. Nanotechnol.* **2020**, *15*, 529.

[7] A. B. Grommet, M. Feller, R. Klajn, *Nat. Nanotechnol.* **2020**, *15*, 256.

[8] H. Chen, J. F. Stoddart, *Nat. Rev. Mater.* **2021**, *6*, 804.

[9] *Handbook of Nanomaterials for Industrial Applications* (Eds: C. M.Hussain), Elsevier, **2018**.

[10] E. Moulin, E. Busseron, N. Giuseppone, CHAPTER 1 Self-assembled Supramolecular Materials in Organic Electronics, in *Supramolecular Materials for Opto-Electronics*, The Royal Society of Chemistry, **2015**, pp. 1-52.

[11] N. Xin, J. Guan, C. Zhou, X. Chen, C. Gu, Y. Li, M. A. Ratner, A. Nitzan, J. F. Stoddart, X. Guo, *Nat. Rev. Phys.* **2019**, *1*, 211.

[12] A. C. Peixoto, A. F. Silva, Smart devices, Micro- and nanosensors, in *Bioinspired Materials for Medical Applications*, (Eds: L. Rodrigues, M. Mota), Woodhead Publishing, **2017**, pp. 297-329.

[13] A. Aviram, M. Ratner, *Chem. Phys. Lett.* **1974**, *29*, 277.

[14] N. Xin, X. Guo, *Chem. Asian J.* **2017**, 373.

[15] P. Gehring, J. M. Thijssen, H. S. J. van der Zant, *Nat. Rev. Phys.* **2019**, *1*, 381.

[16] M. Taniguchi, *Phys. Chem. Chem. Phys.* **2019**, *21*, 9641.

[17] H. Chen, H. Zheng, C. Hu, K. Cai, Y. Jiao, L. Zhang, F. Jiang, I. Roy, Y. Qiu, D. Shen, Y. Feng, F. M. Alsubaie, H. Guo, W. Hong, J. F. Stoddart, *Matter* **2020**, *2*, 378.

[18] E. Coronado, *Nat. Rev. Mater.* **2020**, *5*, 87.

[19] C. W. Fuller, P. S. Padayatti, H. Abderrahim, L. Adamiak, N. Alagar, N. Ananthapadmanabhan, J. Baek, S. Chinni, C. Choi, K. J. Delaney, R. Dubielzig, J. Frkanec, C. Garcia, C. Gardner, D. Gebhardt, T. Geiser, Z. Gutierrez, D. A. Hall, A. P. Hodges, G. Hou, S. Jain, T. Jones, R. Lobaton, Z. Majzik, A. Marte, P. Mohan, P. Mola, P. Mudondo, J. Mullinix, et al., *PANAS* **2022**, *119*, e2112812119.

[20] J. Ulrich, D. Esrail, W. Pontius, L. Venkataraman, D. Millar, L. H. Doerrer, *J. Phys. Chem. B* **2006**, *110*, 2462.

[21] C. Li, I. Pobelov, T. Wandlowski, A. Bagrets, A. Arnold, F. Evers, *J. Am. Chem. Soc.* **2008**, *130*, 318.

[22] S. Martin, I. Grace, M. R. Bryce, C. S. Wang, R. Jitchati, A. S. Batsanov, S. Higgins, C. J. Lambert, R. J. Nichols, *J. Am. Chem. Soc.* **2010**, *132*, 9157.

[23] S. Marques-Gonzalez, D. S. Yufit, J. A. K. Howard, S. Martin, H. M. Osorio, V. M. Garcia-Suarez, R. J. Nichols, S. J. Higgins, P. Cea, P. J. Low, *Dalton Trans.* **2013**, *42*, 338.

[24] H. M. Osorio, S. Martín, D. C. Milan, A. González-Orive, J. B. G. Gluyas, S. J. Higgins, P. J. Low, R. J. Nichols, P. Cea, *J. Mater. Chem.* **2017**, *5*, 11717.

[25] S. V. Aradhya, L. Venkataraman, *Nat. Nanotechnol.* **2013**, *8*, 399.

[26] A. Vilan, D. Aswal, D. Cahen, *Chem. Rev.* **2017**, *117*, 4288.

[27] I. L. Herrer, A. K. Ismael, D. C. Milán, A. Vezzoli, S. Martín, A. González-Orive, I. Grace, C. Lambert, J. L. Serrano, R. J. Nichols, P. Cea, *J. Phys. Chem. Lett.* **2018**, *9*, 5364.

[28] M. El Abbassi, S. Sangtarash, X. Liu, M. L. Perrin, O. Braun, C. Lambert, H. S. J. van der Zant, S. Yitzchaik, S. Decurtins, S.-X. Liu, H. Sadeghi, M. Calame, *Nat. Nanotechnol.* **2019**, *14*, 957.

[29] L. Herrer, A. Ismael, S. Martín, D. C. Milan, J. L. Serrano, R. J. Nichols, C. Lambert, P. Cea, *Nanoscale* **2019**, *11*, 15871.

[30] M. T. González, X. Zhao, D. Z. Manrique, D. Miguel, E. Leary, M. Gulcur, A. S. Batsanov, G. Rubio-Bollinger, C. J. Lambert, M. R. Bryce, N. Agraït, *J. Phys. Chem. C* **2014**, *118*, 21655.

[31] B. Liu, M. Tsutsui, M. Taniguchi, *Micromachines* **2018**, *9*, 282.

[32] M. T. González, A. Díaz, E. Leary, R. García, M. Á. Herranz, G. Rubio-Bollinger, N. Martín, N. Agraït, *J. Am. Chem. Soc.* **2013**, *135*, 5420.

[33] S. Li, J. Li, H. Yu, S. Pudar, B. Li, J. Rodríguez-López, J. S. Moore, C. M. Schroeder, *J. Electroanal. Chem.* **2020**, *875*, 114070.

[34] J. Teyssandier, S. D. Feyter, K. S. Mali, *Chem. Commun.* **2016**, *52*, 11465.

[35] A. Blanco-Gomez, P. Corton, L. Barravecchia, I. Neira, E. Pazos, C. Peinador, M. D. Garcia, *Chem. Soc. Rev.* **2020**, *49*, 3834.

[36] Y. Li, C. Yang, X. F. Guo, *Acc. Chem. Res.* **2020**, *53*, 159.

[37] J. Kramer, R. Kang, L. M. Grimm, L. De Cola, P. Picchetti, F. Biedermann, *Chem. Rev.* **2022**, *122*, 3459.

[38] G. Monta-Gonzalez, F. Sancenon, R. Martinez-Manez, V. Marti-Centelles, *Chem. Rev.* **2022**,

[39] M. Xue, Y. Yang, X. D. Chi, Z. B. Zhang, F. H. Huang, *Acc. Chem. Res.* **2012**, *45*, 1294.

[40] S. Ohtani, K. Kato, S. X. Fa, T. Ogoshi, *Coord. Chem. Rev.* **2022**, 462.

[41] M. Ozmen, A. N. Kursunlu, Y. Acikbas, M. Erdogan, R. Capan, *Applied Physics a-Materials Science & Processing* **2020**, *126*, 212.

[42] M. Wang, S. Fang, S. Yang, Q. Li, N. M. Khashab, J. Zhou, F. Huang, *Mater. Today Chem.* **2022**, *24*, 100919.

[43] X. W. Guan, Q. Lin, Y. M. Zhang, T. B. Wei, J. Wang, Y. Q. Fan, H. Yao, *Soft Matter* **2019**, *15*, 3241.

[44] Y. X. Ni, M. J. Yin, S. Y. Dong, F. H. Huang, Q. Zhao, *Appl. Surf. Sci.* **2020**, *500*, 144056.

[45] Q. Li, Y. Z. Liu, P. R. Liu, L. Q. Shangguan, H. T. Z. Zhu, B. B. Shi, *Org. Chem. Frontiers* **2020**, *7*, 399.

[46] W. W. Feng, M. Jin, K. Yang, Y. X. Pei, Z. C. Pei, *Chem. Commun.* **2018**, *54*, 13626.

[47] K. C. Jie, Y. J. Zhou, E. R. Li, F. H. Huang, *Acc. Chem. Res.* **2018**, *51*, 2064.

[48] E. R. Li, Y. J. Zhou, R. Zhao, K. C. Jie, F. H. Huang, *Ang. Chem. Int. Ed.* **2019**, *58*, 3981.

[49] J. Chen, Y. Wang, C. W. Wang, R. H. Long, T. T. Chen, Y. Yao, *Chem. Commun.* **2019**, *55*, 6817.

[50] Y. Wang, Z. C. Pei, W. W. Feng, Y. X. Pei, *J. Mater. Chem. B* **2019**, *7*, 7656.

[51] T. Ogoshi, T. Kakuta, T. Yamagishi, *Ang. Chem. Int. Ed.* **2019**, *58*, 2197.

[52] L. Y. Guo, J. H. Du, Y. R. Wang, K. Y. Shi, E. Q. Ma, *J. Incl. Phenom. Macrocycl.* **2020**, *97*, 1.

[53] H. Behera, L. Yang, J. L. Hou, *Chin. J. Chem.* **2020**, *38*, 215.

[54] J. F. Chen, J. D. Ding, T. B. Wei, *Chem. Commun.* **2021**, *57*, 9029.

[55] J. J. Li, J. H. Dong, H. Wang, X. Y. Yang, J. Z. Chen, J. L. Gu, S. L. Lin, *Adv. Mater. Interfaces* **2021**, *8*.

[56] L. Zhou, C. Liu, H. C. Zhang, J. Han, Z. N. Liu, *Dies and Pigm.* **2021**, 196.

[57] H. T. Z. Zhu, Q. Li, W. J. Zhu, F. H. Huang, *Acc. Chem. Res.* **2022**, *3*, 658.

[58] P. Demay-Drouhard, K. Du, K. Samanta, X. Wan, W. Yang, R. Srinivasan, A. C. H. Sue, H. Zuilhof, *Org. Lett.* **2019**, *21*, 3976.

[59] T. Zhou, N. Song, H. Yu, Y. W. Yang, *Langmuir* **2015**, *31*, 1454.

[60] L. Luo, G. R. Nie, D. M. Tian, H. T. Deng, L. Jiang, H. B. Li, *Angew. Chem., Int. Ed.* **2016**, *55*, 12713.

[61] T. Ogoshi, S. Takashima, T.-a. Yamagishi, *J. Am. Chem. Soc.* **2015**, *137*, 10962.

[62] S. Dong, B. Zheng, Y. Yao, C. Han, J. Yuan, M. Antonietti, F. Huang, *Adv. Mater.* **2013**, *25*, 6864.

[63] T. Ogoshi, T. Yamagishi, *Chem. Commun.* **2014**, *50*, 4776.

[64] Y. Wang, G. Ping, C. Li, *Chem. Commun.* **2016**, *52*, 9858.

[65] M. Kiguchi, S. Nakashima, T. Tada, S. Watanabe, S. Tsuda, Y. Tsuji, J. Terao, *Small* **2012**, *8*, 726.

[66] W. Zhang, S. Y. Gan, A. Vezzoli, R. J. Davidson, D. C. Milan, K. V. Luzyanin, S. J. Higgins, R. J. Nichols, A. Beeby, P. J. Low, B. Y. Li, L. Niu, *ACS Nano* **2016**, *10*, 5212.

[67] J.-H. Tang, Y. Li, Q. Wu, Z. Wang, S. Hou, K. Tang, Y. Sun, H. Wang, H. Wang, C. Lu, X. Wang, X. Li, D. Wang, J. Yao, C. J. Lambert, N. Tao, Y.-W. Zhong, P. J. Stang, *Nat. Commun.* **2019**, *10*, 4599.

[68] R. Wang, Y. Li, A. Tang, Y. Li, H. Li, *Chem. Commun.* **2022**, *58*, 8290.

[69] R. Chikkaraddy, B. de Nijs, F. Benz, S. J. Barrow, O. A. Scherman, E. Rosta, A. Demetriadou, P. Fox, O. Hess, J. J. Baumberg, *Nature* **2016**, *535*, 127.

[70] N. H. Kim, W. Hwang, K. Baek, M. R. Rohman, J. Kim, H. W. Kim, J. Mun, S. Y. Lee, G. Yun, J. Murray, J. W. Ha, J. Rho, M. Moskovits, K. Kim, *J. Am. Chem. Soc.* **2018**, *140*, 4705.

[71] Q. Lu, K. Liu, H. Zhang, Z. Du, X. Wang, F. Wang, *ACS Nano* **2009**, *3*, 3861.

[72] R. R. Ferradás, S. Marqués-González, H. M. Osorio, J. Ferrer, P. Cea, D. C. Milan, A. Vezzoli, S. J. Higgins, R. J. Nichols, P. J. Low, V. M. García-Suárez, S. Santiago Martín, *RSC Adv.* **2016**, *6*, 75111.

[73] L. M. Ballesteros, S. Martin, S. Marqués-González, M. C. López, S. Higgins, R. J. Nichols, P. J. Low, P. Cea, *J. Phys. Chem.* **2015**, *119*, 784.

[74] B. Xu, N. J. Tao, *Science* **2003**, *301*, 1221.

[75] Y. Tang, Y. Zhou, D. Zhou, Y. Chen, Z. Xiao, J. Shi, J. Liu, W. Hong, *J. Am. Chem. Soc.* **2020**, *142*, 19101.

[76] T. Fu, S. Smith, M. Camarasa-Gómez, X. Yu, J. Xue, C. Nuckolls, F. Evers, L. Venkataraman, S. Wei, *Chem. Sci.* **2019**, *10*, 9998.

[77] X. Li, Q. Wu, J. Bai, S. Hou, W. Jiang, C. Tang, H. Song, X. Huang, J. Zheng, Y. Yang, J. Liu, Y. Hu, J. Shi, Z. Liu, C. J. Lambert, D. Zhang, W. Hong, *Angew. Chem., Int. Ed.* **2020**, *59*, 3280.

[78] R. Frisenda, V. A. E. C. Janssen, F. C. Grozema, H. S. J. van der Zant, N. Renaud, *Nat. Chem.* **2016**, *8*, 1099.

[79] S. Wu, M. T. González, R. Huber, S. Grunder, M. Mayor, C. Schönenberger, M. Calame, *Nat. Nanotechnol.* **2008**, *3*, 569.

[80] C. Wu, D. Bates, S. Sangtarash, N. Ferri, A. Thomas, S. J. Higgins, C. M. Robertson, R. J. Nichols, H. Sadeghi, A. Vezzoli, *Nano Lett.* **2020**, *20*, 7980.

[81] S. Y. Quek, M. Kamenetska, M. L. Stigerwald, H. J. Choi, S. G. Louie, M. S. Hybertsen, J. B. Neaton, L. Venkataraman, *Nat. Nanotechnol.* **2009**, *4*, 230.

[82] A. Magyarkuti, O. Adak, A. Halbritter, L. Venkataraman, *Nanoscale* **2018**, *10*, 3362.

[83] B. Hua, C. Zhang, W. Zhou, L. Shao, Z. Wang, L. Wang, H. Zhu, F. Huang, *J. Am. Chem. Soc.* **2020**, *142*, 16557.

[84] G. Mészáros, C. Li, I. Pobelov, T. Wandlowski, *Nanotechnology* **2007**, *18*, 424004.

[85] C. Sabater, C. Untiedt, J. J. Palacios, M. J. Caturla, *Phys. Rev. Lett.* **2012**, *108*, 205502.

[86] C. Wu, X. Qiao, C. M. Robertson, S. J. Higgins, C. Cai, R. J. Nichols, A. Vezzoli, *Angew. Chem., Int. Ed.* **2020**, *59*, 12029.